PNAS RESEARCH ARTICLE | PSYCHOLOGICAL AND COGNITIVE SCIENCES
NEUROSCIENCE

What can the eye see with melanopsin?

Thomas W. Nugent[a] and Andrew J. Zele[a,1]

Edited by Martin Banks, University of California, Berkeley, CA; received June 3, 2024; accepted October 22, 2024

A subpopulation of human retinal ganglion cells contains the melanopsin photopigment, allowing them to act as a fifth photoreceptor class. These ganglion cells project to the visual cortex, but to reveal its intrinsic contribution to conscious vision is technically challenging as it requires melanopsin to be separated from the responses originating in the rods and three cone classes. Using a display engineered to isolate the melanopic visual response, we show that it detects lowpass spatial (≤0.35 cycles per degree) and temporal image content (≤1 Hz) but cannot reconstruct the stimulus form necessary for object recognition. We demonstrate that a model of the spatially diffuse intrinsically-photosensitive retinal ganglion cells' sampling structure is predictive of the measured image reconstruction limits of melanopic spatial vision. Separately, we find that under five-photoreceptor silent substitution conditions, rod pathways alone can support form vision in bright lighting when typically thought to be in saturation. Form vision that is absent from melanopsin can be only perceived in mixtures of both melanopsin and rod signals because it is the rod pathway that sees the form. Our findings show that melanopsin's unique tuning to the diffuse and slow-changing elements in the world provides a stabilized reference point for vision.

melanopsin | ipRGCs | vision | silent substitution | human

Significance

One subclass of retinal ganglion cells contains a melanopsin photopigment that confers light sensitivity independent of the rod and cone photoreceptors. We show that melanopsin photoreceptors alone are sufficient to produce a visual percept in response to both spatial and temporal patterns. It cannot however reconstruct image form. This evidence suggests that melanopsin is an intrinsic part of how the human eye sees across large areas of visual space and over long durations.

Light-dependent nonvisual functions including circadian photoentrainment, the pupillary reflex, and mood are dependent on intrinsically-photosensitive retinal ganglion cells (ipRGCs) expressing the melanopsin photopigment (1–3). Human vision is best understood in terms of the rod and three cone photoreceptors, with less known about our most evolutionarily ancient photopigment, melanopsin. This photoreceptor's morphology is unique because its photopigment exists within a subclass of retinal ganglion cells (4) and its independent light response extends human vision to a five-photoreceptor model. Present within the ganglion cell's soma and dendrites, melanopsin creates the largest receptive fields in the eye. Contrary to rods and cones, it has a persistent photoresponse to light stimulation (5) and is even capable of tracking day length changes in illumination (6). With its unique traits, melanopic vision can perform functions for which the canonical photoreceptors do not have the tools (7).

Multiple lines of evidence indicate that the melanopsin pathway produces conscious vision (8–10). The initial studies which measured the melanopic visual response were restricted to uniform stimuli with some inherent low spatial frequency, and showed that melanopsin is responsible for signaling brightness (11–14), and has an influence on color perception (9, 10, 15–18). A prior study suggests that spatial patterns may be perceived with melanopic vision (19), but what aspects of image reconstruction are possible have not been reconciled with the anatomy and physiology of melanopsin cells. The lack of knowledge of how melanopsin cells are incorporated into the model of human vision stems from the technical challenge of disentangling its relatively insensitive response from rods and cones. Here, we use our purpose-built display to isolate the intrinsic spatiotemporal characteristics of melanopsin vision. We find that the eye can see spatially structured images with melanopsin, but that melanopic vision cannot resolve the content.

Results

To isolate the visual response of melanopsin, we have developed a display with pixel-level control of five, narrow-band primary lights (Fig. 1*A*, solid curves; *SI Appendix*, Fig. S1) for the purpose of independently modulating the quantal catch of the five photoreceptor classes (melanopsin (i), rhodopsin (R), long (L), middle (M), and short (S) wavelength sensitive cone opsins) at each individual pixel position. This system affords linear control over 768 light levels for each primary (Fig. 1*B*) for measuring threshold level vision and to limit quantization errors in smooth-changing spatiotemporal gratings that would inadvertently lead to artifacts detectable by the eye. The contrast range of the display (19.12%) has the advantage of approaching the limit of maximum possible melanopsin-isolated

Author affiliations: [a]Centre for Vision and Eye Research, Queensland University of Technology, Brisbane, QLD 4059, Australia

Author contributions: T.W.N. and A.J.Z. designed research; performed research; analyzed data; and wrote the paper.

The authors declare no competing interest.

This article is a PNAS Direct Submission.

[1]To whom correspondence may be addressed. Email: andrew.zele@qut.edu.au.

This article contains supporting information online at https://www.pnas.org/lookup/suppl/doi:10.1073/pnas.2411151121/-/DCSupplemental.

Published November 21, 2024.

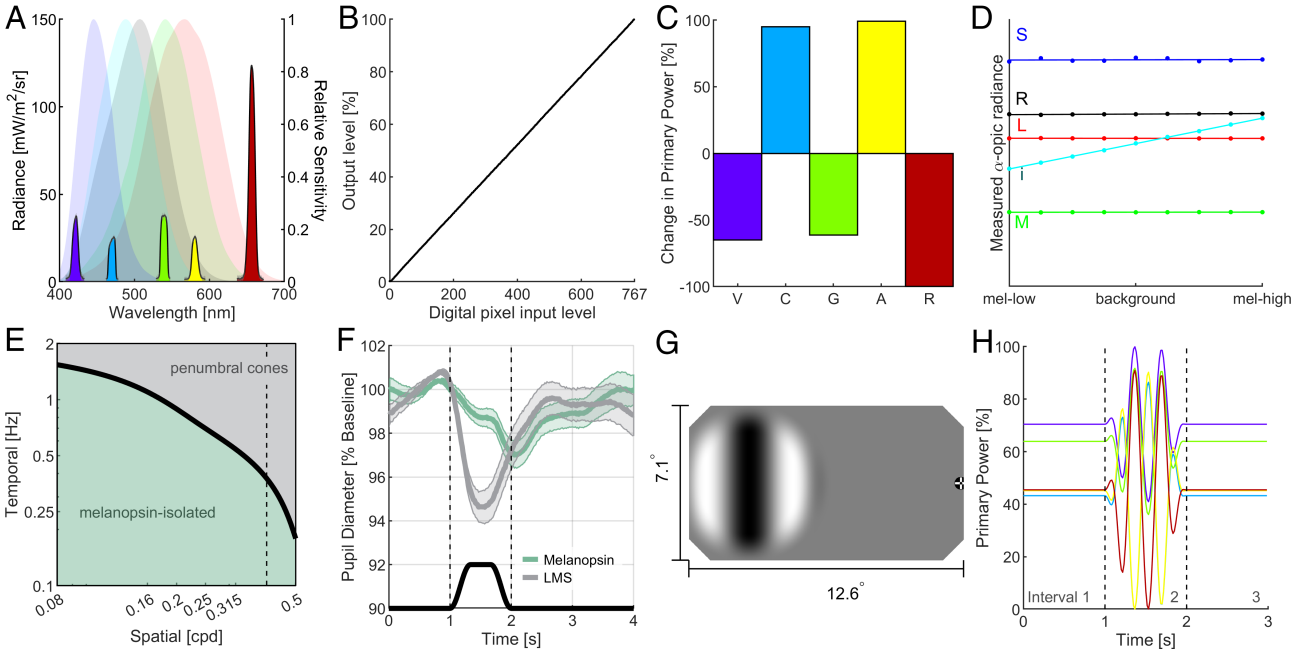

Fig. 1. Isolating melanopsin in humans. (*A*) Spectrum of five primary lights chosen to optimize the achievable melanopsin contrast at equal energy white (solid lines) and CIE 10° Standard Observer spectral sensitivity functions (20) (shaded areas). (*B*) Radiometric output measurements confirm the linear input–output behavior of the five primaries. The mean error between desired input and measured output is 0.074%, roughly half the step size of the 767 input levels. (*C*) Percentage change in primary powers in a maximum contrast melanopsin-isolated stimulus that is invisible to the cone and rod photoreceptors. (*D*) Change in α-opic radiance in melanopsin-isolated stimuli is linear and produces imperceptible changes in the silent rod and cone photoreceptor classes. (*E*) Predicted spatiotemporal range of melanopsin-isolation. Dendritic field diameter of human ipRGCs sets a spatial resolution limit of ≈0.4 cycles per degree (cpd) (vertical dashed line, see *Materials and Methods*). Where the maximum penumbral cone luminance contrast is below the cone visual threshold (21) is the spatiotemporal region where isolated melanopsin visual responses can be measured (green area). (*F*) Pupillometric confirmation (μ ± 95% CI) of melanopsin isolation (green traces) shows a slow and sustained constriction when compared with LMS-cone-isolated pupil responses (gray traces). (*G*) Schematic grating stimulus for measuring spatiotemporal contrast sensitivity. Each grayscale value in the image represents a pixel with a targeted photoreceptor/s excitation achieved by a mixture of the five primary lights and which change overtime as per the standing wave grating shown the adjacent panel. (*H*) Representative temporal changes in the five primary powers during a 3-interval, forced-choice procedure.

contrast in the human eye when measured on an adapting background which is metameric to an equal energy white spectrum (775 photopic Troland for the Commission Internationale de l'Eclairage (CIE) 10° Standard Observer with a 2 mm artificial pupil; 1,295 scotopic Troland). The system's precision in generating melanopsin-isolated stimuli (Fig. 1*C*) is validated by spectroradiometrically measuring the primary outputs as a function of melanopsin contrast across its entire range. No device errors are above threshold when measured at 0.2 cpd, 0.25 HzFig. 3; the maximum open-field rod and cone Michelson contrast errors are *S, M, L, R* = [1.23%, 0.28%, 0.14%, 0.6%] (Fig. 1*D*).

To independently control the spatiotemporal response of all five photoreceptors, we began by estimating the total light seen by a photoreceptor class by correlating its spectrum with the spectral sensitivity of the CIE 10° Standard Observer (20) (Fig. 1*A*, transparent curves). Because each individual participant can differ from the Standard Observer due to a combination of lens aging, macular pigment optical density, opsin polymorphisms, and optical density, the resulting differences in photoreceptor excitations are typically larger than the device errors. We therefore customize our photoreceptor-isolated stimuli to account for these individual differences using a physiological model combined with a minimum motion technique (MMT) (*Materials and Methods*). In addition to calibrating our photoreceptor-isolated stimuli for each participant, we also calculate how the retinal vasculature spectrally filters incoming light and presents a different spectrum to the photoreceptors under the penumbral shadow of the retinal capillaries; these penumbral cones can detect luminance contrasts in nominally cone-silent stimuli (22) (Fig. 1*E*, maximum penumbral cone luminance contrast at 19.12% melanopsin-isolated contrast = 3.3%). Producing photoreceptor-isolated stimuli is a complex task that requires a number of factors to be addressed. We detail how we control for these factors in *SI Appendix*, S1.

In the main experiments, the photoreceptor-directed stimuli were centered at 9° in the temporal retina (Fig. 1*G*) where human ipRGCs have the highest density and smallest dendritic field diameter (23, 24) (≈1.25° of visual angle) and where we expect melanopic vision to have the highest spatial resolution. Importantly, the melanopsin-isolated stimuli produced no perceptible change in the excitations of rhodopsin and the three cone opsins.

As a key external validation of both the precision of the individual observer corrections and an absence of cone intrusions, we measured the pupillary response to a melanopsin-directed stimulus (Fig. 1*F*). This pupillary light response shows the signature slow pupil constriction (peak constriction amplitude: 3.0%, time to peak: 1.05 s, constriction velocity: 2.8% · s^{-1}) and sustained post-illumination pupil response (PIPR at 1s: 1.1%), whereas the LMS-cone isolated pupillary light response has a rapid constriction (peak constriction amplitude: 5.4%, time to peak: 0.5 s, constriction velocity: 10.8% · s^{-1}) and redilation prior to stimulus offset (PIPR at 1 s: 0.6%) (25). The absence of a fast pupillary constriction at stimulus onset adds to the weight of evidence that the melanopsin-isolated stimuli do not have cone intrusions—though it is possible for the visual threshold of intruding cone signals to be below the respective pupillary response threshold.

Melanopsin Can Detect Low Spatiotemporal Frequencies at High Contrast. To determine whether the eye can see spatial variations with melanopsin, we asked whether observers (*Materials and Methods*) could detect which interval (of three) contained a melanopsin-isolated, spatiotemporal grating (Fig. 1 *G* and *H*).

Using this detection paradigm, we titrated the threshold contrast using a double-alternating staircase procedure for each spatial and temporal frequency pair. For each observer, we measured four repeats of each staircase to find the average threshold contrast, with more than 100 gratings at different contrasts shown to each observer for each spatiotemporal frequency (Fig. 2*A*, μ ± 95% CI). From the average threshold detection contrasts within the melanopsin-isolated region, we created a model of the melanopic spatial detection response at each temporal frequency. The model we used was a Gaussian function commonly used to describe the spatial sensitivity of receptive field structures (26) (solid lines, Fig. 2*A* and Dataset S1).

This model showed that detection with melanopic vision has a prominent combined low pass sensitivity to both spatial (≤0.2 to 0.25 cpd) and temporal (≤1 Hz) frequencies (Fig. 2*B*). A two-way ANOVA of a linear mixed-effect model showed that contrast detection thresholds differed significantly with spatial ($F_{1,141} = 20.72$, $P = 1.1 \times 10^{-5}$) and temporal frequencies ($F_{1,141} = 33.3$, $P = 5 \times 10^{-8}$). Peak contrast sensitivity of this melanopic response (7%, 10%, 13%, and 14.5% Michelson contrast for the observers; Fig. 2*C*) occurs at the lowest spatiotemporal frequencies measured (0.08 cpd; 0.1 Hz or 0.25 Hz) and from the extrapolated model can see up to a maximum spatial frequency of 0.35 cpd.

To investigate whether the observed melanopic spatial response was consistent with ipRGC anatomy, we used the receptive field structure of ipRGCs (i.e., soma positions and template cell shapes labeled in human donor retinae) (23, 24) to reconstruct the gratings at different spatial frequencies (Code S2). This simulation (*SI Appendix*, Fig. S3 and Movie S1) shows the ipRGC anatomy provides a fundamental limit to melanopic spatial vision (i.e., cell spacing, nonuniform cell distribution, diffuse sampling across cells, and overlapping dendritic fields between adjacent cells). A modulation transfer function was created from the reconstructed gratings (*SI Appendix*, Fig. S2) which showed that at spatial frequencies above 0.6 cpd, a 19.12% contrast melanopsin grating would be reconstructed by ipRGCs as less than 8.8% contrast—which is the average detection threshold of melanopsin where it is most sensitive. This places an anatomical upper limit on melanopic spatial vision.

Visual Percepts Arising from Melanopsin. For each spatiotemporal frequency, we asked the observers to describe the visual percept. Observers reported that melanopic gratings were perceived as spatially chaotic visual patterns, as opposed to the sinusoidal gratings presented (Fig. 1*G*). These spatially chaotic patterns are present in our simulated reconstruction using ipRGC distribution maps from donor eyes (*SI Appendix*, Fig. S3). Fixation loss during stimulus presentation led to the disappearance of the grating percept even at suprathreshold melanopsin contrasts. Following refixation, it took time to recover the grating percept, consistent with the slow and sustained spiking pattern of melanopsin cells. If this were a cone-mediated process, the eye movements would convert the spatial structure into temporal contrast and improve

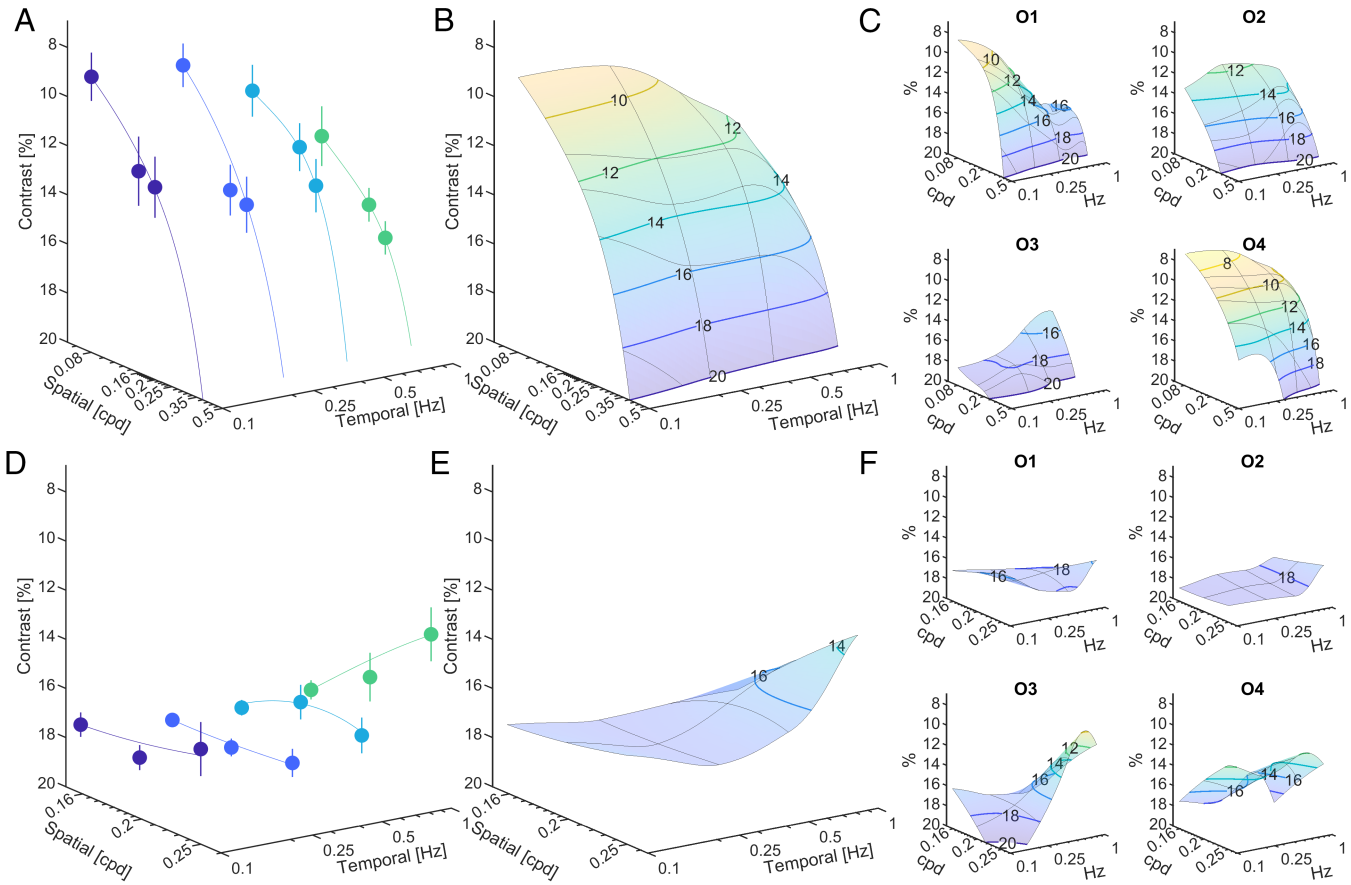

Fig. 2. Melanopsin-isolated spatiotemporal contrast thresholds. (*A*) Melanopic spatial detection functions (μ ± 95% CI, n = 3 observers; O1, O2, O4) with best-fitting difference of Gaussian's model. (*B*) Three-dimensional melanopic spatiotemporal threshold surface with a modified Akima cubic Hermite interpolation. (*C*) Individual melanopic spatiotemporal threshold detection surfaces (n = 4). (*D*) Melanopic spatial identification functions (μ ± 95% CI, n = 4 observers) are flat, and at the instrument gamut limit. (*E*) Three-dimensional melanopic identification surface interpolated as per panel *B*. (*F*) Individual melanopic identification threshold surfaces, where the spatiotemporal low pass structure is not present for any observer.

detection, contradictory to what was observed (27). Melanopsin-isolated lights were also described as fluorescent, which can be associated with the brightness signaling of the melanopsin pathway (12, 13), and with a shared hue described as ranging from a sand-like faint yellow (O1 and O4)/orange (O2) with increased melanopsin to a faint cyan (similar to a clear sky) with the decreased melanopsin activation within the grating. At the spatiotemporal frequencies that we predicted cones within the penumbral shadow of the retinal vasculature could perceive luminance contrast from the spectral filtering of the primary lights (>0.25 cpd, >1 Hz) (Fig. 1*H*, *SI Appendix*, Fig. S4, and Code S1), all observers reported a shift to an achromatic grating appearance denoting the transition from melanopsin driving the percept to a combination of melanopsin and intruding cones.

Melanopsin Has No Form Vision. Having established that melanopic vision can detect low spatiotemporal frequency patterns (Fig. 2*B*), we asked whether this spatial response contributes to the conscious perception of a grating's form? To test this, we presented the same grating stimuli, but instead, we now asked observers to identify the orientation of the melanopsin-isolated, spatiotemporal grating (two alternative forced choice: horizontal or vertical). The mean orientation identification threshold within the melanopsin-isolated egion for each stimulus pair shows a flat response near the instrument's maximum contrast (Fig. 2 *D* and *E* and Dataset S1), without the low pass structure which was present with the detection task (Fig. 2*A*). A two-way ANOVA showed no significant effect of spatial or temporal frequency on threshold contrast in the melanopsin-isolated region. No observer could reliably discriminate the grating orientation across any of the melanopsin-isolated, spatiotemporal frequencies measured (Fig. 2*F*).

Our system presented melanopsin Michelson contrasts up to 19.12% near the limit of human melanopic vision under silent substitution. We could not reject the null hypothesis that observers could not identify the melanopsin grating orientation at any melanopsin contrast (one-tailed, two-sample *t* test, t(122) = -0.882, $P = 0.19$) and found the standard error of the mean (SEM) identification threshold contrast in the melanopsin-isolated region ($\mu = 17.18\%$, SEM = 0.42%) spanned the expected mean of the staircase procedure if participant responses were random ($\mu_0 = 17.41\%$). We conclude from the statistical analysis that there is no evidence that form vision arises from melanopsin.

We also measured the observer's identification contrast sensitivity at spatiotemporal frequencies outside the melanopsin-isolated region and where vision includes penumbral and other accumulated cone intrusions (*SI Appendix*, Fig. S4). These measurements show that the detection and identification contrast thresholds converge at higher spatial (0.5 cpd) and temporal (2 Hz) frequencies showing that intruding cone vision can reconstruct image form, unlike melanopsin. Notably, there is a steeper drop in sensitivity in the identification task compared with the detection task when transitioning from the penumbral cone region to the melanopsin-isolated region (Fig. 1*E* and *SI Appendix*, Fig. S4 *A* and *B*), suggesting that melanopsin stimulation can aid cone vision in the detection task.

Rhodopsin and Melanopsin Signals Are Mutually Inhibitory During Silent Substitution. Our instrumentation was designed to control rods because a growing body of evidence indicates that they are operational in photopic light levels commonly used in this type of work, and especially so under conditions of silent substitution where all cone signals are silenced (28, 29). To investigate whether rods can mediate a detectable visual percept at the photopic level of our study (equivalent to 1,295 scotopic Td), we measured the rod-isolated threshold at a spatiotemporal frequency near the peak melanopsin detection sensitivity (0.2 cpd, 0.25 Hz). The classic study of rod thresholds over intensity found that the rod threshold at our light level was in the range of 105 to 420% Weber contrast (approximately 34 to 67% Michelson contrast) (30). We found that photopic rod vision under silent substitution has a contrast threshold in the range of 6 to 8% Michelson contrast. This rod threshold is near the S-cone isolated threshold and is more sensitive than for melanopsin (Fig. 3*A*).

To determine how photopic rod signaling influences melanopic vision in four-photoreceptor silent substitution paradigms (i.e., cones silent, melanopsin and rhodopsin modulated in phase), we presented stimuli that simultaneously contained both melanopsin and rhodopsin contrast in different ratios. If rod and melanopsin signals do not interact, the supplemental rod contrast will not affect the melanopsin threshold. When a simultaneous, subthreshold rod contrast was presented we found no clear change in the melanopsin threshold contrast, whereas suprathreshold rod contrasts inhibited melanopsin contrast sensitivity with 1% supplemental, suprathreshold rod contrast correspondingly increased melanopsin threshold contrast by 2% (Fig. 3*B*).

Melanopic Vision Exists Where Cones Are Least Sensitive. To contextualize visual detection with melanopsin, we compared its detection threshold with traditional cone mechanisms near the peak melanopsin detection sensitivity. This comparison (Fig. 3*A*) shows that isolated melanopic vision is the least sensitive visual mechanism, requiring ≈13% melanopsin contrast to detect the presence of a 0.2 cpd, 0.25 Hz spatiotemporal grating. As expected at the low spatiotemporal frequency measured, human eyes have higher sensitivity to L-M cone opponent isolated stimuli (Fig. 3*A*) than to cone luminance isolated stimuli (31, 32). We also sought to explore where melanopic vision is localized within the spatiotemporal plane of cone vision, by repeating our detection paradigm for LMS-cone isolated stimuli. This achromatic cone detection surface follows the same structure and peak spatiotemporal frequency response as represented by Kelly (21). We find that the melanopic detection thresholds localize to the lowest frequencies in a range where the achromatic cone detection threshold surface is least sensitive (Fig. 3*C*).

Discussion

This work provides the foundation for understanding the functional role of melanopsin in conscious visual perception, separate from responses originating in the rod and cone pathways. We isolated the melanopic spatiotemporal response of the human eye using a display technology developed explicitly to control the excitations of all five photoreceptors in the human eye at a single pixel level. With the ability to send an isolated melanopsin stimulus, we show that melanopic vision can detect light containing spatiotemporal contrast information, but paradoxically, melanopsin does not create form vision sufficient to identify the image structure. We also find that rods can support form vision in photopic lighting in conditions of cone silent substitution, and when combined with melanopsin, the rod stimulation reestablishes the lost image structure, but at the expense of reduced visual sensitivity. This effect on spatial vision extends prior reports that rods can perceive uniform, flickering stimuli at photopic light levels and inhibit melanopsin sensitivity to these flickering stimuli when presented temporally in-phase (28).

Melanopsin's inability to reconstruct an image may stem from the anatomical structure of human ipRGCs. Because lossless image reconstruction requires at least two samples per spatial frequency (i.e., the Nyquist frequency), ipRGC spacing will constrain lossless visual reconstruction to spatial frequencies below

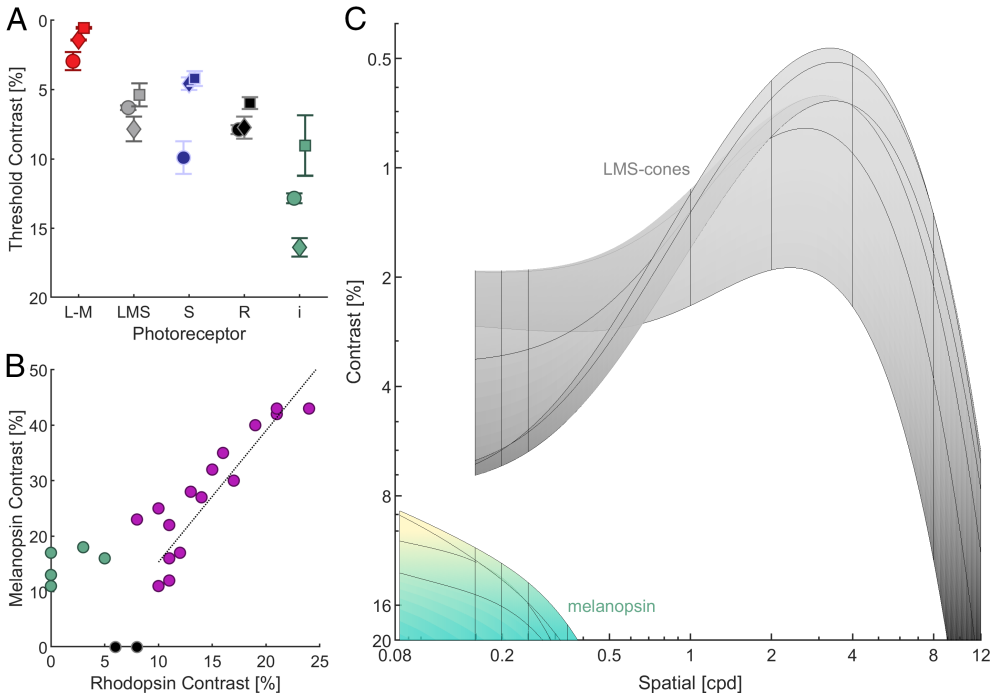

Fig. 3. Comparison of melanopsin visual sensitivity with rod and cone photoreceptors. (*A*) Detection thresholds of low spatiotemporal frequency photoreceptor-isolated gratings near the peak sensitivity of melanopsin (0.2 cpd, 0.25 Hz; μ ± 95% CI). (*B*) Detection thresholds of melanopsin-directed gratings with supplemental rod contrast (black: rod-isolated; green: melanopsin + subthreshold rod; magenta: melanopsin + suprathreshold rod). (*C*) Detection threshold surface of melanopsin-isolated vision (yellow to cyan) compared with LMS-cone isolated vision (gray). In each surface, the intersections of the horizontal (Hz) and vertical line traces (cpd) specify the locations of the measured spatiotemporal data.

0.6 cpd, on average (*Materials and Methods* and *SI Appendix*, Figs. S2 and S3). We show that humans can detect melanopsin-isolated, spatial frequencies below 0.35 cpd (Fig. 2*B*) with a spatial percept matching the broadband spatial noise described in aliased cone signals (33). Notably, our psychophysical data correspond with physiological measurements of the spatial profile and cutoff frequency (0.4 to 0.5 cpd) of ipRGCs' extrinsic response in nonhuman primates (4). The melanopic spatial resolution limit is therefore 170× lower than foveal cone vision (34) (up to 60 cpd), suggesting that if it has a role in vision, it would be to represent large-scale content within the visual field. Our observations could potentially be explained by one subtype mediating melanopic vision, perhaps the inner-stratifying ipRGCs (visualization in *SI Appendix*, Fig. S3). Alternatively, if the entire population of ipRGCs contributes to what the eye can see with melanopsin, the lower visual resolution is likely driven by the overlapping dendritic fields (24) which diffusely sample and integrate spatial information over larger retinal areas than predicted by the Nyquist limit. From the average dendritic field size in the retinal position tested (375 μm mean diameter), we can infer that only spatial frequencies ≤0.39 cpd would be signaled by adjacent, nonoverlapping ipRGCs which are required to not artificially reduce the signaled contrast through cells signaling mutual spatial information (*SI Appendix*, Figs. S2 and S3 and Movie S1).

Accompanying the melanopic spatial detection is a shared fluorescent and hue percept. If melanopsin has a role in color vision, it would be best placed to track changes of the spectral power distribution of sunlight across the day. The reported hue percept may be used in this sense to "yellow-shift" our color perception at cooler color temperatures (e.g., a bluish-appearing daylight spectrum) while "blue-shifting" warmer color temperatures (e.g., an orangish-appearing sunset spectrum). This observed percept agrees with the extrinsic S-cone OFF and L+M cone ON inputs to ipRGCs in nonhuman primates (4, 35) and psychophysical measurements under five photoreceptor silent substitution that describes the hue as yellow at higher melanopsin levels (15, 18, 36), with our finding describing the faint cyan hue associated with a melanopsin decrement.

One observer had a divergent hue and brightness percept; except for a faint bluish percept at the lowest temporal frequency of 0.1 Hz, it was described as achromatic with no fluorescence at the other measured spatiotemporal frequencies. The lack of shared melanopsin percepts in this observer explains their lower contrast sensitivity to all spatiotemporal frequencies without exhibiting the prominent low pass characteristic (Fig. 2*C*, O3). This observer's insensitivity to melanopsin-isolated lights might be explained by anatomical differences in ipRGC retinal density as evident in human donor eyes (*Materials and Methods* and *SI Appendix*, Fig S2), but importantly, an absence of intruding visual signals highlights the ability of the display system to produce cone- and rod-silent spatiotemporal stimuli within our melanopsin-isolated, spatiotemporal region. As a result of this participant's lack of shared melanopic percepts, their detection data were excluded from averaged melanopsin detection data (Fig. 2*A*).

The traditional view of rod saturation is drawn from Aguilar and Stiles (30) who measured rod increment threshold across a broad range of light levels. They found that at lower illuminations (0.01 to 100 scotopic Td), rods had a constant threshold in the range 13 to 34% Weber contrast (approximately 6 to 14% Michelson contrast). Beyond 100 scotopic Trolands, the sharp increase in rod threshold was inferred as its approach to saturation. Interestingly, our measurements found that at 1,295 scotopic Td the rods could see a 6 to 8% threshold Michelson contrast. This measured photopic rod threshold matches the expected sensitivity of the rod pathway in scotopic/mesopic conditions, suggesting that rods have a way of seeing photopic stimuli if that stimulus does not contain any cone modulations within it (albeit with some constant cone content in the adapting background).

There is a precedent for expecting rod-initiated vision at higher photopic illuminations (up to at least 2,000 ph Td) from studies using uniform fields devoid of spatial structure (28, 29). Higher illuminations are known to promote faster rod kinetics in the macaque retina (37) and rod bipolar cells remain responsive during electroretinographic recordings in humans (38). These photopic rod-initiated signals can impact both melanopsin- and cone-mediated temporal visual processing (28). Although we have measured rod vision in photopic lighting, this does not necessarily preclude rod saturation occurring at light levels higher than used in this study.

Only two approaches exist to target melanopsin-mediated spatial vision in trichromatic humans, being silent substitution using a four- or five-photoreceptor model. These approaches differ only in whether they consider rhodopsin excitation as a potential confounding artifact in the melanopsin-directed stimulus during silent substitution. For the four-photoreceptor model, this requires an assumption that rods are saturated at photopic light levels, which has only been demonstrated in nonsilent substitution conditions [i.e., rod signals are unmeasurable in the presence of concomitant cone signals (30)]. To investigate the difference between four- and five-photoreceptor models of silent substitution, we tested what supplemental rod contrast does to melanopsin contrast sensitivity (Fig. 3*B*). We found supplemental, suprathreshold rod contrast in a melanopsin-directed light inhibits its visual sensitivity. Because melanopsin and rhodopsin spectral sensitivities are highly correlated, most four photoreceptor models have significant suprathreshold rod contrasts at melanopsin contrasts above threshold. This may explain how data measured with a four-photoreceptor model find form vision, whereas we find no evidence of form vision with melanopsin.

Only one other study has evaluated form vision with melanopsin. Using a four-photoreceptor framework, Allen and colleagues (19) measured a spatial visual response to a combined melanopsin and rod stimulus (19% melanopsin contrast with 14% rod contrast for the CIE 10° Standard Observer). They conclude from their measurements that melanopsin can see and identify grating orientations up to a spatial frequency of ≈1.5 cpd. In the retinal region measured in their study, the ipRGC density of 13 cells·mm^{-2} corresponds to a Nyquist frequency of 0.49 cpd; the inner-stratifying ipRGCs have a lower cell density and Nyquist frequency (≈8 cells·mm^{-2}, 0.38 cpd; *Materials and Methods*). Given the anatomical constraints that ipRGCs place on spatial resolution, it is probable that the measurements in ref. 19 originate from a photoreceptor class which more densely tiles the retina (i.e., the unconstrained rods or cone intrusion). Alternatively, their larger field (15° diameter) might represent stimulus form by recruiting more ipRGCs (≈194 vs. 64 cells in this study), enabling participants to infer a likely orientation from the chaotic spatial pattern perceived. However, this mechanism would still not enable melanopic vision to identify a grating's orientation at spatial frequencies beyond its anatomical limits (≫0.38 cpd) or the spatial detection limits measured here (>0.4 cpd).

Conclusion

Melanopsin can see low spatial and temporal frequencies as a chaotic spatial pattern with the increment perceived as a fluorescent yellowish-orangish and the decrement appearing cyanish. The way it perceives these frequencies is unique in that melanopic vision is capable of detecting spatial patterns, but this detection does not translate to an ability to identify the pattern orientation. Our findings have implications for how ipRGCs innervate within the visual cortex and suggest that they are sparsely represented in areas with orientation selectivity. The presence of melanopsin-driven spatial responses indicates that all five photoreceptor types can contribute to our visual representation. As the world we see is mostly constructed of low spatial and temporal elements, melanopic vision is uniquely tuned to provide our vision with a stabilized reference.

Materials and Methods

Five-Primary Display. A five-primary, Maxwellian view display (*SI Appendix*, Fig. S1) was custom built to independently control the excitations of the melanopsin, rhodopsin, and three cone opsins (L, M, and S) in the human eye (39). This five-primary display is created by optically merging five, independently controlled projectors that each project a single, narrowband primary image plane. The primaries were selected with peak wavelengths (±full-width at half-maximum bandwidth) of 420 nm (10 nm), 470 nm (10 nm), 540 nm (10 nm), 570 nm (10 nm), and 650 nm (10 nm) (Fig. 1*A*) to maximize the melanopsin-isolated contrast (Dataset S2).

All experiments were conducted with reference to an adapting background metameric to an equal-energy white (EEW) spectrum (CIE $x,y,z = [1/3,1/3,1/3]$) (Fig. 1 *C* and *D*). Using the method of silent substitution (Fig. 1*C*), the system can achieve a maximum isolated melanopsin Michelson contrast of 19.12% with rods and cones silenced. This approaches the limit of the maximum possible melanopsin-isolated contrast on a background metameric to an EEW background in the human eye; which is 20.23% with any set of narrowband (10 nm FWHM) primaries (39) (note that not all primaries are commercially available). The five projectors are centrally controlled with a field programmable gate array to ensure temporal synchrony across projectors. Each primary display has ≈9.5 bits of linear control per pixel (Fig. 1*B*) in a 60 Hz video frame to enable measurement of threshold level vision, with a pixel resolution of 360 × 640 pixels and the projected image subtends a visual angle of 7.1° × 12.6°.

Stimuli are generated on a controlling computer in MATLAB using a combination of Psychtoolbox (40) and custom developed OpenGL graphics shaders. Device calibrations are carried out as described in ref. 41, including primary output linearization, spatial alignment of projectors, spatial homogenization of projector outputs, and temporal alignment of interprimary video frames.

General Stimulus Specification. Melanopsin-directed gratings are measured at each combination of six spatial frequencies (0.08, 0.167, 0.2, 0.25, 0.35, and 0.5 cpd) and five temporal frequencies (0.1, 0.25, 0.5, 1, and 2 Hz). Cone luminance-directed (L+M+S) stimuli are measured at a broader range of spatial frequencies (0.167, 0.2, 0.35, 1, 2, 4, 8, and 12 cpd) and temporal frequencies (0.1, 0.25, 1, 2, 8, and 16 Hz) because cones support a larger range of visual responses. Red-green chromatic, S-cone, rod, and combined melanopsin- and rod-stimuli are measured at a single spatiotemporal frequency of 0.25 Hz and 0.25 cpd near the peak sensitivity of melanopsin (but away from their respective peak sensitivities at higher frequencies) to compare their contrast sensitivity to melanopsin under the same conditions.

The test stimuli are a standing-wave grating (Fig. 1 *E* and *F*) which oscillates following the function:

$$\vec{p}\,(x,y,t) = \vec{p}_{\,B} + \Delta\vec{p} \times \frac{m}{M}\sin\left(2\pi f_t t\right) \cdot \cos\left(2\pi f_s\left[x\cos(\theta)+y\sin(\theta)\right]\right), \quad [1]$$

where $\vec{p}_{\,B}$ are the primary powers which produce the chosen background adapting chromaticity (39, 41), $\Delta\vec{p}$ is the change in primary powers which silently modulate the target photoreceptor, m is the contrast and M is the maximum achievable contrast, f_s is the spatial frequency in cycles per degree (cpd), and f_t is the temporal frequency in Hertz (Hz). The lowest measured spatial frequency (0.08 cpd) was a temporal modulation of the entire 6° field. At the lowest spatial frequencies, the interaction between the spatial grating and the limits of the field size produces some residual DC modulation of the melanopsin signal. These residual DC melanopsin modulations remain below melanopsin threshold (0.167 cpd = 1.2%, 0.2 cpd = 0%, and 0.25 cpd = 0.86% melanopsin-isolated, Michelson contrast).

The test gratings are spatially windowed by a circular 6° raised cosine and presented against a uniform, EEW background with a retinal illuminance of 775 Td for the CIE 10° Standard Observer (equivalent to 246 cd/m^2 with a 2mm artificial pupil) (Fig. 1*E*). To limit fixation losses, the marker was a bullseye and cross hair shape (42) (ABC shape). The fixation position located the center of the stimuli at 9°

in the temporal retina and outside of the macular pigment where the eccentricity-dependent exponential decline in its optical density approaches zero (43).

Six photoreceptor-directed stimulus combinations were generated using the methods described in ref. 41: We first used five-primary, silent substitution to generate melanopsin-isolated (i) stimuli producing no change in the excitation of rhodopsin and the three cone opsins (Fig. 1*D*). To compare the spatiotemporal response of melanopsin to cone vision, we then measured L-, M-, and S-cone stimuli modulated in a 2/3:1/3:1 in-phase cone ratio to produce cone luminance-(L+M+S) directed stimuli with no change in the excitation of rhodopsin and melanopsin (i.e., cone-isolated stimuli). Having identified the peak melanopic response, we examine the relative sensitivity of red-green color vision using an L- and M-cone modulated in a 2/3:1/3 ratio in counterphase with no change in S-cones, rhodopsin, and melanopsin; the blue-yellow dimension of chromatic vision with S-cone isolated stimuli (no change in rhodopsin, melanopsin, or L- and M-cone excitations); and rod-isolated photopic vision (no change in L-, M-, and S-cone or melanopsin excitations); the latter determines whether rods can be ignored in light-adapted, silent substitution protocols with four- or five-photoreceptor models. Finally, to understand the interaction type between rhodopsin and melanopsin in silent substitution, we measured combined melanopsin- and rod-directed stimuli in variable ratios, modulated in-phase (with no change in cone excitation) with conditions designed to emulate prior four-photoreceptor methodologies (i.e., melanopsin lights which contain a concomitant rod contrast signal).

Confirmation of the Device's Melanopsin Isolation. To confirm the precision of the isolation, spectroradiometric measurements (EPP2000C50 μm Slit UV-VIS Spectrometer, StellarNet, Tampa, FL) of full-field, melanopsin-isolated stimuli were taken at nine equidistant intervals between the melanopsin-minimum and -maximum (Fig. 1*D*). The Standard Observer's photoreceptor excitations were calculated for each of the stimulus conditions. The device's rod and cone contrast errors reflect a combined measurement of both the actual photoreceptor excitation errors and the fluctuating background spectral noise in the spectroradiometer (which is most prominent at short wavelength for the given spectroradiometer), indicating the actual device errors are likely lower than these measured values.

Penumbral Cone Contrast. Visual sensitivity to cone luminance signals is bandpass to both spatial and temporal frequencies (21), with decreasing contrast sensitivity at lower spatiotemporal frequencies. As a result of the spectral filtering of the primary lights by the retinal vasculature, we estimated the transition spatiotemporal frequencies (Fig. 1*E*) wherein the luminance contrast in a melanopsin-isolated light may become visible to cones in their penumbral shadow (22) due to their higher contrast sensitivity than melanopsin. The spectral filtering of the penumbral shadow of the retinal vasculature is estimated as

$$\alpha_{total}(\lambda) = 0.85\alpha_{HbO_2}(\lambda) + 0.15\alpha_{Hb}(\lambda), \quad [2]$$

where the absorbance coefficients of oxyhemoglobin $\alpha_{HbO2}(\lambda)$ and deoxyhemoglobin $\alpha_{Hb}(\lambda)$ are estimated by

$$\alpha_i = \frac{dc \cdot \ln(10)}{m}\varepsilon(\lambda), \quad [3]$$

where $\varepsilon_i(\lambda)\,\mathrm{cm}^{-1}/(\mathrm{mol/L})$ is the molar extinction coefficient for hemoglobin (44), $d = 5 \times 10^{-4}$ cm is the average capillary diameter in the retina (45), $c = 150$ g/L is a typical concentration of hemoglobin in blood, and $m = 64{,}500$ g/mol is the molar concentration of hemoglobin (44).

The luminance contrast signal available to penumbral cones in the CIE Standard Observer (20) at the maximum 19.12% melanopsin contrast was estimated to be 0.8%, and after accounting for individual differences in preretinal filtering was estimated for each observer as; O1: 2.9%, O2: 3.1%, O3: 3.3%, and O4: 2.1%. As the luminance contrast scales proportionally with melanopsin contrast, these values are lower at the measured melanopsin thresholds. By comparing the individual observer's penumbral cone intrusions to the luminance spatiotemporal threshold surface (21), we predict that melanopsin measurements are free from penumbral cone intrusions <1.3 Hz at 0.1 cpd, <0.8 Hz at 0.2 cpd, <0.65 Hz at 0.25 cpd, <0.5 Hz at 0.315 cpd, and <0.1 Hz at 0.5 cpd (Fig. 1*E*, the black line is this model prediction; Code S1). In the rod-isolated stimuli, the luminance contrast visible to penumbral cones at the maximum 8.41% rod contrast is ≤3.9% for all observers, which means penumbral cone intrusions are subthreshold at the single 0.25 Hz, 0.2 cpd rod-isolated spatiotemporal frequency measurement.

Psychophysical Procedures. The capacity for the melanopsin pathway to detect the presence of a spatiotemporal grating was first determined to establish the contrast detection limits of melanopsin vision. Gratings were randomly presented in one interval of a 3-interval, forced-choice paradigm. The observer is instructed to indicate in which interval the stimuli was present via a button press on a handheld gamepad. Each interval is presented for 1 s (or $1/f_t$ seconds if longer). An identification task was then performed to determine whether the anatomical and physiological properties of ipRGCs can support spatiotemporal form vision. Gratings were presented in one of two orientations (horizontal or vertical) and the observer was instructed to identify the direction of the presented grating in a 2-alternative, forced-choice paradigm. For both tasks, the temporal frequency was randomized in a single session measured at one spatial frequency. Participants were asked to describe the visual percepts associated with the stimuli. The contrast sensitivity of a spatiotemporal pair is titrated with a double random alternating staircase procedure (46). A minimum of four repeats of each staircase procedure are reported for each spatiotemporal pair. The number of errors at maximum stimulus contrast was recorded to indicate whether the threshold could not be seen within the instrument gamut.

Testing sessions were ≈1 h in duration, beginning with a 15-min preadaptation period to the darkened laboratory. To limit any effect of circadian variation on melanopsin-mediated function, all observers completed their session at a similar time each day (47). Psychophysical paradigms began after a minimum 2 min light adaptation to the steady illumination. Psychophysical testing was conducted monocularly with the right eye and a natural pupil through a 2 mm artificial pupil. Observer responses were recorded using a handheld gamepad. Breaks were provided when required to minimize fatigue.

Participants. All experimental protocols were conducted in accordance with a Queensland University of Technology Human Research Ethics Committee approval (no. 1700000510) and followed the tenets of the Declaration of Helsinki; written informed consent was obtained from all participants. The four experienced psychophysical observers (all male) who participated in the study (ages: 30 to 47) were healthy and with trichromatic color vision (Ishihara pseudoisochromatic plates and L'anthony Desaturated D-15 Test). Ophthalmic screening determined that all participants have a visual acuity of 0.0 log-MAR (6/6) or better, age-normal spatial contrast sensitivity [Combined Spatial Contrast and Visual Acuity chart (48)], no ocular diseases as confirmed with ophthalmoscopy, fundus photography (Canon Non-Mydriatic Retinal Camera, CR-DGi, Canon Inc., Tokyo, Japan), optical coherence topography (RS-3000 OCT RetinaScan Advance, Nidek Co., Ltd., Tokyo, Japan), and intraocular pressure measurement (<21 mmHg) (iCare IC100; Icare Finland Oy, Vantaa, Finland), and have no systemic disease. In addition to the ophthalmic screening, the observers were individually calibrated and then completed a high volume of samples per condition (n ≈ 100) across 1,072 staircase procedures, for more than 26,800 detection/identification measurements, which equated to ≈100 h of active testing.

Individual Observer Calibrations. The study of human vision through melanopsin is conducted with reference to a standardized set of five photoreceptor action spectra and inert ocular prereceptoral lens and macular pigment filtering (CIE S026 2018). To avoid errors arising from differences between an individual and the CIE 10° Standard Observer due to preretinal filtering, each participant completed individual observer calibrations across the five primaries using the MMT (49) positioned at the same retinal eccentricity as the experimental measurements. The calibration stimulus was a 1 cpd, 15 Hz square wave grating windowed by a circular 6° Gaussian set against a homogeneous 120 Td background adapting field metameric to an EEW spectrum. The point of minimum motion is the equiluminant condition of each primary relative to a reference (green). This equiluminant condition differs between observers and with respect to the CIE 10° Standard Observer spectral sensitivity functions due to an individual's preretinal filtering and L:M cone ratios.

Using the range of physiologically possible lens ages, macular pigment optical densities, L- and M-cone polymorphisms, and L:M cone ratios, we simulate the spectral sensitivity differences between each set of physiological parameters and

the CIE 10° Standard Observer. With the different sets of plausible spectral sensitivities, we calculate the equiluminant condition in the MMT for each potential set of physiological parameters. A least squared errors model is then created to match our measured MMT coefficients with these simulated individual differences. An individual's L:M cone ratios and opsin polymorphisms affect the spectral sensitivity of the L+M luminance mechanism with no effect on the spectral sensitivity of S-cones, rods, and melanopsin, while an individual's preretinal filtering (lens and macular pigment optical density) affects the spectral sensitivity of all photoreceptor classes. To account for this, we inverse the effect of the modeled L:M cone ratio on the measured MMT coefficients so that the cone ratios do not affect the calculated excitation of the remaining photoreceptor classes. We find that these MMT measurements and least squared model adjustment accurately predict the lens ages of all participants.

Eye Fixation Tracking and Pupillometric Confirmation of Melanopsin Isolation. After individual observer calibrations, melanopsin- and cone-directed pupillometry was conducted to confirm photoreceptor isolation (25). Consensual pupil responses from the left eye were recorded under infrared illumination 640 × 480 pixels; 60 Hz; Point Gray FMVU-03MTM-CS; Richmond, BC, Canada; Computar TEC55 55mm telecentric lens, Computar, Cary, NC, USA) in response to a 1 s, photoreceptor-isolated raised-cosine pulse with a 10-s interstimulus interval to allow pupils to return to their baseline. Matching the main experiments, the stimulus was a circular 6° field, windowed by a 2D raised-cosine and centered at 9° in the temporal retina. A minimum 40 trials were recorded. Post hoc filtering was used to remove pupil recordings with blink artifacts or fixation loss according to standard procedures (50). Eye movement data were recorded using the same pupil imaging system. Fixation was tracked by finding the centroid of the ellipse which best fit the edge of the recorded pupil during stimulus presentation. The fixation data indicate stable fixation with a standard deviation in pupil position of 0.307 mm.

Anatomical Prediction of ipRGC Spatial Contrast Sensitivity. In the retinal region measured (6 to 12° temporal eccentricity, 1.75 to 3.50 mm temporal retina), anatomical studies (23, 24) of human donor eyes determined that ipRGCs have an average dendritic field diameter of ≈375 μm and retinal density of ≈18 to 22 ipRGCs·mm^2. As the melanopsin chromophore is present throughout the soma and across its large dendritic field, a single ipRGC therefore provides a spatially diffuse image sample. The dendritic fields of adjacent ipRGCs overlap so that they integrate mutually shared spatial information. Together the spatially diffuse sample and overlapping dendritic fields act to reduce the spatial contrast perceived by ipRGCs when the spatial frequencies are not less than those which allow adjacent dendritic fields to independently signal both the peak and trough of the spatial grating; we therefore predict the spatial frequency below which ipRGCs should have their peak spatial sensitivity:

$$f_{peak} = \frac{0.291}{2d_{ipRGC}} = 0.39 \text{ cpd}, \quad [4]$$

where f_{peak} is the spatial frequency that does not require the adjacent signaling ipRGCs to have overlapping dendritic fields when centered on the peak and trough of the spatial stimulus, and d_{ipRGC} is 0.375 mm, which is the average diameter of ipRGCs within our stimulus field (24).

The retinal density of ipRGCs will predict the spatial frequencies that aliasing noise will interfere with an observer's ability to perceive spatial contrast. Although for simplicity we assume uniform retinal tiling, it is important to recognize that ipRGC tiling is nonuniform with localized regions of higher and lower density even on the scale of adjacent ipRGCs (23, 24). This feature of ipRGC anatomy predicts localized regions of nonuniform spatial contrast sensitivity within a stimulus grating at spatial frequencies near the calculated Nyquist frequency. The implication of the retinal density of ipRGCs for melanopic vision is that contrast sensitivity will be reduced at spatial frequencies above the ipRGC Nyquist frequency:

$$f_{Nyquist} = \left(\frac{2}{0.291} \cdot \sqrt{\frac{2}{\sqrt{3}D_{ipRGC}}} \right)^{-1} = 0.60 \text{ cpd}, \quad [5]$$

where $f_{Nyquist}$ is highest frequency that can be reconstructed without aliasing noise assuming a circularly bandlimited stimulus, both inner- and outer-stratifying ipRGCs contribute to a melanopic visual response, all ipRGCs of an ipRGC subtype innervate the lateral geniculate nucleus, uniform hexagonal ipRGC distribution and point source sampling (which is not true as discussed above). D_{ipRGC} is the retinal density of ipRGCs in our stimulus field, which is approximately 20 cells mm^{-2} (figure 9 from ref. 24), and the scalar value of 1/0.291 converts between mm on the retina and visual angle in cpd. Code for anatomical predictions is available in Code S2.

Data, Materials, and Software Availability. All study data are included in the article and/or supporting information.

ACKNOWLEDGMENTS. We thank Beatrix Feigl, Drew Carter, and Prakash Adhikari for their constructive discussions. This work was supported by an Australian Research Council Future Fellowship ARC-FT180100458 (A.J.Z.).

1. S. Hattar, H.-W. Liao, M. Takao, D. M. Berson, K.-W. Yau, Melanopsin-containing retinal ganglion cells: Architecture, projections, and intrinsic photosensitivity. *Science* **295**, 1065–1070 (2002).
2. A. D. Güler *et al.*, Melanopsin cells are the principal conduits for rod–cone input to non-image-forming vision. *Nature* **453**, 102–105 (2008).
3. T. A. LeGates *et al.*, Aberrant light directly impairs mood and learning through melanopsin-expressing neurons. *Nature* **491**, 594–598 (2012).
4. D. M. Dacey *et al.*, Melanopsin-expressing ganglion cells in primate retina signal colour and irradiance and project to the LGN. *Nature* **433**, 749–754 (2005).
5. A. Liu *et al.*, Encoding of environmental illumination by primate melanopsin neurons. *Science* **379**, 376–381 (2023).
6. K. Y. Wong, A retinal ganglion cell that can signal irradiance continuously for 10 hours. *J. Neurosci.* **32**, 11478–11485 (2012).
7. D. S. Joyce, K. W. Houser, S. N. Peirson, J. M. Zeitzer, A. J. Zele, "Melanopsin vision: Sensation and perception through intrinsically photosensitive retinal ganglion cells" in *Elements in Perception*, J. T. Enns, Ed. (Cambridge University Press, 2022), pp. 1–68, 10.1017/9781009029865.
8. F. H. Zaidi *et al.*, Short-wavelength light sensitivity of circadian, pupillary, and visual awareness in humans lacking an outer retina. *Curr. Biol.* **17**, 2122–2128 (2007).
9. H. Horiguchi, J. Winawer, R. F. Dougherty, B. A. Wandell, Human trichromacy revisited. *Proc. Natl. Acad. Sci. U.S.A.* **110**, E260–E269 (2013).
10. M. Spitschan *et al.*, The human visual cortex response to melanopsin-directed stimulation is accompanied by a distinct perceptual experience. *Proc. Natl. Acad. Sci. U.S.A.* **114**, 12291–12296 (2017).
11. T. DeLawyer, S. Tsujimura, K. Shinomori, Relative contributions of melanopsin to brightness discrimination when hue and luminance also vary. *J. Opt. Soc. Am. A* **37**, A81–A88 (2020).
12. T. M. Brown *et al.*, Melanopsin-based brightness discrimination in mice and humans. *Curr. Biol.* **22**, 1134–1141 (2012).
13. A. J. Zele, P. Adhikari, B. Feigl, D. Cao, Cone and melanopsin contributions to human brightness estimation. *J. Opt. Soc. Am. A* **35**, B19–B25 (2018).
14. M. Yamakawa, S. Tsujimura, K. Okajima, A quantitative analysis of the contribution of melanopsin to brightness perception. *Sci. Rep.* **9**, 1–8 (2019).
15. A. J. Zele, B. Feigl, P. Adhikari, M. L. Maynard, D. Cao, Melanopsin photoreception contributes to human visual detection, temporal and colour processing. *Sci. Rep.* **8**, 1–10 (2018).
16. P. A. Barrionuevo, C. P. Filgueira, D. Cao, Is melanopsin activation affecting large field color-matching functions? *J. Opt. Soc. Am. A* **39**, 1104–1110 (2022).
17. T. DeLawyer, K. Shinomori, Melanopsin-driven surround induction on the red/green balance of yellow. *J. Opt. Soc. Am. A.* **40**, A40–A47 (2023).
18. D. Cao, A. Chang, S. Gai, Evidence for an impact of melanopsin activation on unique white perception. *J. Opt. Soc. Am. A.* **35**, B287–B291 (2018).
19. A. E. Allen, F. P. Martial, R. J. Lucas, Form vision from melanopsin in humans. *Nat. Commun.* **10**, 1–10 (2019).
20. Commission Internationale de l'Eclairage, "CIE System for metrology of optical radiation for ipRGC-influenced responses to light" (CIE S 026/E:2018, International Commission on Illumination, CIE Central Bureau, Vienna, Austria, 2018).
21. D. H. Kelly, Motion and vision. II. Stabilized spatio-temporal threshold surface. *J. Opt. Soc. Am.* **69**, 1340–1349 (1979).
22. M. Spitschan, G. K. Aguirre, D. H. Brainard, Selective stimulation of penumbral cones reveals perception in the shadow of retinal blood vessels. *PLoS One* **10**, e0124328 (2015).
23. H.-W. Liao *et al.*, Melanopsin-expressing ganglion cells on macaque and human retinas form two morphologically distinct populations. *J. Comp. Neurol.* **524**, 2845–2872 (2016).
24. S. Nasir-Ahmad, S. C. S. Lee, P. R. Martin, U. Grünert, Melanopsin-expressing ganglion cells in human retina: Morphology, distribution, and synaptic connections. *J. Comp. Neurol.* **527**, 312–327 (2019).
25. A. J. Zele, P. Adhikari, D. Cao, B. Feigl, Melanopsin and cone photoreceptor inputs to the afferent pupil light response. *Front. Neurol.* **10**, 529 (2019).
26. R. W. Rodieck, Quantitative analysis of cat retinal ganglion cell response to visual stimuli. *Vision Res.* **5**, 583–601 (1965).
27. A. Casile, J. D. Victor, M. Rucci, Contrast sensitivity reveals an oculomotor strategy for temporally encoding space. *Elife* **8**, e40924 (2019).
28. S. Uprety, P. Adhikari, B. Feigl, A. J. Zele, Melanopsin photoreception differentially modulates rod- and cone-mediated human temporal vision. *iScience* **25**, 104529 (2022), 10.1016/j.isci.2022.104529.
29. A. G. Shapiro, Cone-specific mediation of rod sensitivity in trichromatic observers. *Invest. Ophthalmol. Vis. Sci.* **43**, 898–905 (2002).
30. M. Aguilar, W. S. Stiles, Saturation of the rod mechanism of the retina at high levels of stimulation. *Opt. Acta (Lond.)* **1**, 59–65 (1954).

31. A. Chaparro, C. F. Stromeyer, E. P. Huang, R. E. Kronauer, R. T. Eskew, Colour is what the eye sees best. *Nature* **361**, 348–350 (1993).
32. A. B. Watson, H. B. Barlow, J. G. Robson, What does the eye see best? *Nature* **302**, 419–422 (1983).
33. D. R. Williams, N. J. Coletta, Cone spacing and the visual resolution limit. *J. Opt. Soc. Am. A* **4**, 1514–1523 (1987).
34. F. W. Campbell, D. G. Green, Optical and retinal factors affecting visual resolution. *J. Physiol.* **181**, 576–593 (1965).
35. S. S. Patterson, J. A. Kuchenbecker, J. R. Anderson, M. Neitz, J. Neitz, A color vision circuit for non-image-forming vision in the primate retina. *Curr. Biol.* **30**, 1269–1274.e2 (2020).
36. P. A. Barrionuevo, M. L. Sandoval Salinas, J. M. Fanchini, Are ipRGCs involved in human color vision? Hints from physiology, psychophysics, and natural image statistics. *Vis. Res.* **217**, 108378 (2024).
37. W. N. Grimes, J. Baudin, A. W. Azevedo, F. Rieke, Range, routing and kinetics of rod signaling in primate retina. *Elife* **7**, e38281 (2018).
38. A. M. Cameron, L. Miao, R. Ruseckaite, M. J. Pianta, T. D. Lamb, Dark adaptation recovery of human rod bipolar cell response kinetics estimated from scotopic b-wave measurements. *J. Physiol.* **586**, 5419–5436 (2008).
39. T. W. Nugent, A. J. Zele, A five-primary Maxwellian-view display for independent control of melanopsin, rhodopsin, and three-cone opsins on a fine spatial scale. *J. Vis.* **22**, 20 (2022).
40. M. Kleiner *et al.*, What's new in Psychtoolbox-3. *Perception* **36**, 1–16 (2007).
41. T. W. Nugent *et al.*, Protocol for isolation of melanopsin and rhodopsin in the human eye using silent substitution. *STAR Protoc.* **4**, 102126 (2023).
42. L. Thaler, A. C. Schütz, M. A. Goodale, K. R. Gegenfurtner, What is the best fixation target? The effect of target shape on stability of fixational eye movements. *Vis. Res.* **76**, 31–42 (2013).
43. B. R. Hammond, B. R. Wooten, D. M. Snodderly, Individual variations in the spatial profile of human macular pigment. *J. Opt. Soc. Am. A* **14**, 1187–1196 (1997).
44. S. Prahl, *Optical Absorption of Hemoglobin* (Oregon Medical Laser Center, 1999).
45. D. M. Snodderly, R. S. Weinhaus, J. C. Choi, Neural-vascular relationships in central retina of macaque monkeys (Macaca fascicularis). *J. Neurosci.* **12**, 1169–1193 (1992).
46. T. N. Cornsweet, The staircase-method in psychophysics. *Am. J. Psychol.* **75**, 485–491 (1962).
47. A. J. Zele, B. Feigl, S. S. Smith, E. L. Markwell, The circadian response of intrinsically photosensitive retinal ganglion cells. *PLoS One* **6**, e17860 (2011).
48. P. Adhikari, D. D. Carter, B. Feigl, A. J. Zele, Design and validation of a chart-based measure of the limits of spatial contrast sensitivity. *Ophthalmic Physiol. Opt.* **42**, 110–122 (2022).
49. S. M. Anstis, P. Cavanagh, "A minimum motion technique for judging equiluminance" in *Colour Vision: Physiology and Psychophysics*, J. D. Mollon, L. T. Sharpe, Eds. (Academic Press, 1983), pp. 155–166.
50. C. Kelbsch *et al.*, Standards in pupillography. *Front. Neurol.* **10**, 129 (2019).